Microstructure Knowledge Systems for Capturing Process-Structure Evolution Linkages

David B. Brough[a], Daniel Wheeler[b], James Warren[b], Surya R. Kalidindi[a,c,*]

[a] *School of Computational Science and Engineering, Georgia Institute of Technology, Atlanta, GA 30332, USA*
[b] *Materials Science and Engineering Division, Material Measurement Laboratory, National Institute of Standards and Technology, Gaithersburg, MD 20899, USA*
[c] *George W. Woodruff School of Mechanical Engineering, Georgia Institute of Technology, Atlanta, GA 30332, USA*

*Corresponding author
Email address: surya.kalidindi@me.gatech.edu (Surya R. Kalidindi)
URL: http://davidbrough.net (David B. Brough), http://wd15.github.io/about (Daniel Wheeler), http://www.ctcms.nist.gov/~jwarren/ (James Warren)

Abstract

This paper develops and demonstrates a novel data science framework for capturing and communicating critical information regarding the evolution of material structure in spatiotemporal multiscale simulations of various processing operations employed by the manufacturing industry. This new framework is essentially an extension of the MKS (Materials Knowledge Systems) framework that was previously demonstrated for capturing microstructure-property linkages in spatial multiscale simulations. Furthermore, this paper presents a derivation of the MKS framework using different basis functions, and explores their potential benefits in establishing the desired process-structure-property (PSP) linkages. These developments are demonstrated using a Cahn-Hilliard simulation, where structure evolutions were predicted three orders of magnitude faster than an optimized numerical integration algorithm. This study suggests that the MKS localization framework provides an alternate method to learn the underlying embedded physics in a numerical model expressed as Green's function based influence kernels rather than differential equations, and potentially has computational advantages in problems where numerical integration schemes are challengingare challenging to optimize. With this extension, we have now established a comprehensive framework for capturing PSP linkages for spatiotemporal multiscale materials modeling and simulations.

Keywords: Materials Knowledge Systems, Spectral Representations, Cahn-Hilliard model, Phase Field, Structure Evolution, Multiscale Modeling
2015 MSC: 00-01, 99-00

1. Introduction

Customized materials design (including the design of a manufacturing process route) resulting in the combination of properties desired for a specific application is a highly challenging inverse problem, owing mainly to the extremely large parameter space involved in defining the hierarchical internal structure of the material. However, this endeavor has great potential for impacting virtually all emerging technologies [1–11], with significant economic consequences. The central impediment comes from the need to consider the relevant details of the hierarchical internal structure (spanning a multitude of length scales) that control the properties of interest to a specific application. Additionally, a diverse range of coupled physical phenomena occur at different timescales at each of the different length scales. Therefore, one is generally daunted by the enormous difficulty involved in tailoring the material structure to yield desired combinations of properties or performance characteristics.

Historically, and mainly because of the difficulties mentioned above, materials development efforts have relied largely on experimentation. Consequently, many of the efforts aimed at designing and developing new/improved materials have incurred significant cost and time. Recent advances in physics-based modeling of multiscale materials phenomena [12–21] have raised the exciting possibility that the vast design space for experimentation can be constrained to a significant degree by embracing in-silico simulations and explorations. In other words, there is a tremendous potential for significant reductions in cost and time incurred in materials development effort if one could judiciously utilize multiscale materials modeling and simulation tools in combination with a reduced number of experiments.

The central impediments associated with the effective utilization of physics-based multiscale materials models in the materials development efforts have been summarized in recent review articles [18, 22]. An important strategy in addressing these impediments involves the formulation and utilization of robust surrogate models (also called metamodels or emulators) for computationally

efficient communication of critical information between well separated structure/length/time scales. Such low-dimensional, but sufficiently accurate, models present a computationally viable approach for exploring the extremely large materials design space.

In the context of hierarchical materials (with details of the material structure spanning multiple well-separated scales) surrogate models are needed to exchange high value information in both directions between the scales. Depending on the direction of information flow, the models can be classified as homogenization (information flowing from lower scales to higher scales) or localization (information flowing from higher scales to lower scales) relationships. It should be noted that localization linkages are significantly more difficult to establish compared to the homogenization linkages; indeed the latter are implicitly embedded within the former and can be recovered when needed. The recently formulated Materials Knowledge Systems framework (MKS) provides a data-driven approach for creating robust surrogate models for the localization relationships [20, 23–26].

MKS creates accurate localization relationships by merging concepts from the physics-based statistical continuum theories developed by Kroner [27, 28], machine learning [29–31] and digital signal processing [32]. The MKS localization relationship takes the form of a Volterra series expansion involving convolutions of physics-capturing kernels (based on well established concepts of Green's functions) with hierarchical microstructure descriptors. These kernels (referred to as influence functions) capture and organize the governing physics as convolution operators that are independent of the microstructure descriptors. Therefore, in the MKS approach, these kernels are calibrated using a set of data-driven protocols in a one-time effort. Once the kernels are calibrated and validated, they can be used to predict the local responses for new microstructures at very minimal computational expense. Consequently, these MKS kernels are of tremendous utility in any multiscale materials modeling/simulation efforts.

Prior effort in MKS was largely focused on structure-property localization linkages expressed as computationally efficient metamodels (i.e., surrogate mod-

els or emulators). The current effort is aimed at the extension and application of the MKS approach to include spatiotemporal process-structure evolution linkages. In general, the process-structure evolution linkages are significantly harder to establish compared to the structure-property linkages, because of the need to explicitly account for the time evolution of the important field quantities (in addition to their spatial distributions), many of which demand continuous descriptions. Consequently, there currently exist only a few reports in literature describing efforts aimed at capturing the salient process-structure evolution metamodels for multiscale materials phenomena. One area that has received a lot of attention in prior literature is the evolution of crystallographic texture in deformation processing of polycrystalline metals [33–45]. However, in this set of applications, all the attention is generally focused on capturing the salient details of the time evolution, while ignoring or grossly simplifying the spatial distribution of the important field variables involved. More recently, there have been a limited number of efforts aimed at mining low-dimensional process-structure evolution linkages from results accumulated in phase-field simulations [21, 21, 46–48]. In these prior applications, gross simplifications were made either by limiting the set of initial microstructures or microstructure descriptors, or by selecting rudimentary representations of the local states involved.

In this paper, we extend the MKS framework to allow efficient capture of the process-structure evolution localization linkages in one large time step (or multistep). Indeed, this extension when suitably combined with the existing MKS framework has the potential to facilitate a common, consistent, broadly applicable, framework for casting all of the relevant process-structure-property (PSP) linkages in a selected class of materials. A second major thrust of this paper is derivation of the MKS framework using spectral representations for some of the main functions (kernels) involved in these linkages. To the best of our knowledge, this paper represents the first demonstration of the potential benefits that could accrue from using these spectral representations in arriving at highly compact, accurate, low-computational cost, high value, surrogate models for process-structure evolution linkages over large time domains. The novel

protocols described above are demonstrated in this paper through a specific case study involving the extraction of process-structure evolution linkages embedded in the simulation results produced by a selected phase-field model.

2. Generalized MKS Framework for Process-Structure Linkages

The development of the generalized MKS framework for process-structure linkages will be presented here using the Cahn-Hilliard model as an example. However, the generalized final expression formulated here is broadly applicable to various other microstructure evolution models. The Cahn-Hilliard description of microstructure evolution can be expressed as [49]

$$\frac{\partial \phi(x,t)}{\partial t} = D\nabla^2\Big(\big[\phi(x,t)(1-2\phi(x,t)^2\big] + \gamma\nabla^2\phi(x,t)\Big) \tag{1}$$

In Eq. (1), $\phi(x,t)$ is an order parameter used to represent the concentration field at location x and time t, $\sqrt{\gamma}$ represents the interface width, and D is the diffusivity. Note also that a double well potential with minima at -1 and 1 has been used in Eq. (1) for the free energy term [50, 51].

The theoretical framework of MKS is built on perturbation expansions. For the present case, we therefore start by expressing the concentration field $\phi(x,t)$ in terms of a reference quantity $\bar{\phi}$ (constant in both space and time) and a local perturbation $\phi'(x,t)$ from that reference as

$$\phi(x,t) = \bar{\phi} + \phi'(x,t) \tag{2}$$

Introducing Eq. (2) into Eq. (1) results in the following differential equation.

$$\begin{aligned} \frac{\partial \phi'}{\partial t} - D\nabla^2\phi' &= D\nabla^2\Big(\gamma\nabla^2\phi' - \big[3\phi'\bar{\phi}^2 + 3\phi'^2\bar{\phi} - \phi'^3\big]\Big) \\ &= D\nabla^2\Big(\gamma\nabla^2\phi' + \psi(x,t)\Big) \end{aligned} \tag{3}$$

We can use a Green's function approach to find the solution to Eq. (3) where

$$\frac{\partial G(x-x',t-t')}{\partial t} - D\nabla_x^2 G(x-x',t-t') = \delta(x-x',t-t') \tag{4}$$

and with a suitable change of variables we have

$$\begin{aligned}\phi'(x,t) = &-\int_V G(r,t)\phi'(x-r,0)dr+ \\ &\int_T\int_V G(r,\tau)D\nabla_r^2\Big(\gamma\nabla_r^2\phi'(x-r,t-\tau)+\psi(x-r,t-\tau)\Big)drd\tau\end{aligned} \tag{5}$$

In Eq. (5), $\phi'(x,0)$ is the initial value of the perturbed concentration. Assuming periodic boundary conditions, the operators ∇_r can be moved from concentration terms to the Green's functions.

$$\begin{aligned}\phi'(x,t) = &-\int_V G(r,t)\phi'(x-r,0)dr+ \\ &\int_T\int_V D\gamma\nabla_r^4 G(r,\tau)\phi'(x-r,t-\tau)+D\nabla_r^2 G(r,\tau)\psi(x-r,t-\tau)drd\tau\end{aligned} \tag{6}$$

Recursive substitution of $\phi'(x,t)$ into equation (6) produces a series (called the weak contrast expansion) that can be used to compute the perturbed concentration field [27, 28, 52, 53].

$$\phi'(x,t) = -\int_V\Big[1-\int_T\int_V\tilde{G}(r,r',t,\tau)dr'd\tau\Big]G(r,t)\phi'(x-r,0)dr+... \tag{7}$$

with

$$\tilde{G}(r,r',t,\tau) = D\nabla_r^2\Big[\nabla_r^2 G(r',\tau)\gamma-3\bar{\phi}^2 G(r',\tau)\Big] \tag{8}$$

Simplified analytical solutions for Eqs. (7) and (8) are very difficult and demand highly sophisticated approaches to handle the convergences of the terms in the series [54, 55]. There have also been numerous approaches utilizing numerical iterative schemes to solve the same equations [56–61]. The numerical approaches generally demand significant computational resources because of the highly nonlinear expressions embedded in Eqs. (7) and (8). More importantly, most conventional numerical approaches do not facilitate learning. In other words, when the equations are solved for one specific set of inputs there is no established formalism for transferring the knowledge gained in the process to the next application of the same set of equations for a different set of inputs. This is precisely where data science approaches, such as the MKS approach, bring many potential benefits. In the data science approach, we recognize that each term in the series is essentially a convolution, where the kernel is completely

independent of the topological details of the material microstructure. Suitable algorithms are then designed and employed to efficiently learn these kernels from previously accumulated results. In many ways, the calibrated MKS linkages take full advantage of the known physics of the phenomena, and supplement only the mathematically intractable components with data science approaches, where they exhibit a decisive advantage.

The MKS kernels facilitate learning and transfer of knowledge to a new set of microstructure inputs. In order to accomplish this, Eqs. (7) and (8) need to be reformulated using the concepts of microstructure function and local states [62, 63]. The local state captures all the attributes (thermodynamic state variables) needed to identify the physical properties to be assigned to the spatiotemporal location of interest in the material internal structure. In the problem described here, either the concentration value or the perturbed concentration value (after selecting a reference concentration value) can serve as local state variables. The local state will be denoted as h. The set of all values that h can take is denoted as the local state space, H. The main distinction between h and ϕ' (or ϕ) is that the later is a specific value assigned to a specific spatiotemporal location, while the former denotes any value that could have been assigned to the later.

The introduction of the concept of the local state now allows us to describe a microstructure function $m(h, x, t)$ as the probability density associated with finding the local state h at spatial position x at time t. The expectation value obtained using this probability density distribution (on the local state space) should be taken as the specific value assigned in the fully deterministic framework described earlier. In other words, for the fully deterministic case, one could write $m(h, x, t) = \delta(h - \phi'(x, t))$. For the more general case, the definitions introduced above lead to the following mathematical statements

$$\int_H m(h, x, t) dh = 1 \tag{9}$$

$$\phi'(x, t) = \int_H h m(h, x, t) dh \tag{10}$$

The introduction of the microstructure function as a probability density function brings the added benefit that it maps complex descriptions of local state (potentially could be a combination of several scalar and tensor thermodynamic state variables) into a continuous scalar-valued function that lends itself naturally to spectral representations [64–67]. Extending the treatment above to the term containing the Green's function in Eq. (7) allows us to define an influence function or localization kernel as

$$\alpha(h,r,t) = -h\Big[1 - \int_T \int_V \tilde{G}(r,r',t,\tau)dr'd\tau\Big]G(r,t) \tag{11}$$

Recasting Eq. (7) with the terms defined in Eq. (10) and (11) takes the following form.

$$\phi'(x,t) = \int_V \int_H \alpha(h,r,t)m(h,x-r,0)dhdr + ... \tag{12}$$

The derivation of Eq. (12) is a key step in the formulation of the MKS approach for the process-structure evolution localization linkages sought in this work. The main benefit of the form of Eq. (12) lies in the fact that $\alpha(h,r,t)$ serves as a convolution kernel capturing all of the relevant physics in the problem, and operates on the initial microstructure function $m(h,x-r,0)$. Even more importantly, when the series is expanded properly, the localization kernel is completely independent of the microstructure function $m(h,x,0)$. Furthermore, Eq. (12) is the exact analogue of the structure-property localization linkages established previously in the MKS framework [20, 23–26]. Therefore, the extension presented here now makes it possible to explore the complete set of process-structure-property linkages in a consistent MKS framework in both space and time.

Because of the specific way in which Eq. (12) was derived, it is relatively easy to write the additional terms in the series expansion. For example, the second term in this expansion would be expressed as

$$\int_H \int_H \int_V \int_V \int_T \alpha(h,h',r,r',t,t')m(h,x-r,0)m(h',x-r',0)dhdh'drdr'dt' \tag{13}$$

Therefore, another way to interpret the series expansion in Eq. (12) is to recognize that each term in the series captures the contribution arising from a specific

arrangement of the local microstructure in the neighborhood of the spatial voxel of interest as a function of time.

The next step in the practical implementation of the MKS framework is to transform Eq. (12) into a discrete representation. In other words, the functions $\phi'(x,t)$, $\alpha(h,x,t)$ and $m(h,x,t)$ need to be discretized. Following notations and conventions employed in signal processing [68, 69], we will use round brackets to represent variables with continuous domains and square brackets to represent variables with discrete domains.

The discrete version of $\phi'(x,t)$ is denoted as $p[s,n]$; these are formally related to each other as

$$\frac{1}{\Delta x \Delta t}\int_s\int_n \phi'(x,t)dxdt = p[s,n] \tag{14}$$

In Eq. (14), s and n enumerate uniformly partitioned intervals that fully span the continuous domains of space V and time T, respectively, and Δx and Δt denote appropriate measures of the intervals. Therefore, the discrete version of $\phi'(x,t)$ essentially captures the averaged values within the uniformly subdivided intervals in space within the time step n.

Functions $\alpha(h,x,t)$ and $m(h,x,t)$ exhibit a dependence on the local state variable, in addition to the spatial and temporal variables. The spatial and temporal variables are discretized using the same method outlined in Eq. (14), but there are two potential strategies to deal with the discretization of these functions with respect to the local state variable. The simplest approach is to discretize the local state space H is to use triangle or hat basis functions $\Lambda(h-l)$ to divide the local state space into intervals. The hat basis functions are defined in Eq. (15).

$$\Lambda(h-l) = max\left(1 - \left|\frac{h(L-1)}{H} - \frac{Hl}{L-1}\right|, 0\right) \tag{15}$$

In Eq. (15), L is the total number of hat basis functions used to span the local state space and l enumerates the hat functions. H and h maintain their definitions as the local state variable and local state space respectively. The hat functions are placed along the local state space such that the highest and

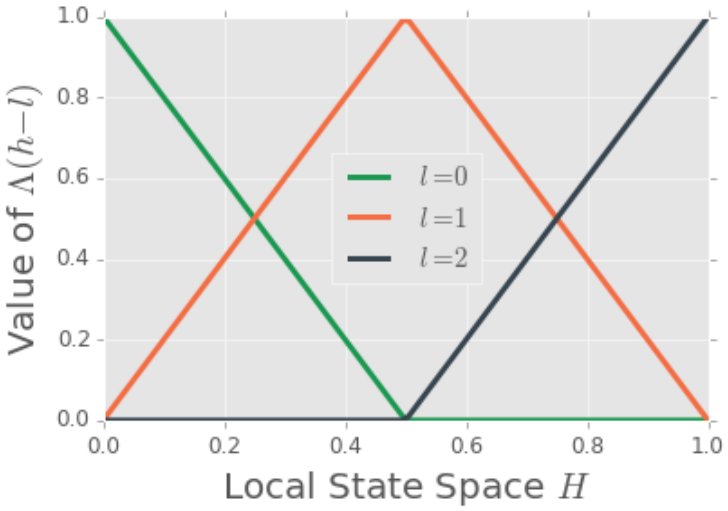

Figure 1: Three hat basis functions Λ used to discretize the local state space H. This method is referred to as Primitive basis functions.

lowest values of the local state space fall on the peak values of the hat functions associated with the highest and lowest values of l. An example of these hat functions with $L = 3$ and $h \in [0, 1]$ is found in Fig. 1. Using this method to position the hat functions in the local state space H ensures the sum of all hat functions contained within the local state space sum to 1, and that a summation of the hat functions times the microstructure function returns the original microstructure function.

$$\sum_{l=0}^{L-1} \Lambda(h-l) = 1; h \in H \tag{16}$$

$$\sum_{l=0}^{L-1} \Lambda(h-l) m(h,x,t) = m(h,x,t) \tag{17}$$

In previous work [48], this approach has been referred to as Primitive binning using the Primitive basis functions [20, 23–26] leading to

$$\frac{1}{\Delta x \Delta t} \int_H \int_s \int_n \Lambda(h-l) m(h,x,t) dx dt dh = m[l,s,n] \tag{18}$$

$$\frac{1}{\Delta x \Delta t} \int_H \int_s \int_n \Lambda(h-l)\alpha(h,x,t)dxdtdh = \alpha[l,s,n] \tag{19}$$

where l now enumerates the number of basis functions used to represent the local state variable h. This primitive binning approach results in the MKS formulation that is consistent with most of the prior studies [20, 23–26], where it is expressed as

$$p[s,n] = \sum_{r=0}^{S-1} \sum_{l=0}^{L-1} \alpha[l,r,n]m[l,s-r,0] + ... \tag{20}$$

Alternatively, the functions on the local state space can be represented to adequate accuracy using highly efficient Fourier basis functions. For example, it is well known that orthonormal functions developed through classical Sturm-Liouville theory can be used as basis functions in many applications. Using such basis functions, one can establish representations such as the ones shown below for an arbitrary function [70–73]:

$$f(h) = \sum_{l=-\infty}^{\infty} c_l \xi_l(h) \tag{21}$$

$$\frac{1}{N_l} \int_a^b \xi_{l'}(h)\xi_l(h)w(h)dh = \delta_{ll'} \tag{22}$$

In Eq. (22) ξ_l is the l^{th} order orthonormal basis function, $w(h)$ is the weighting function, $\delta_{ll'}$ is the Kronecker delta and N_l is a normalization constant that depends on the order and type of the basis functions. The most important feature of Eq. (21) is that the set of coefficients c_l now provide a discrete representation of the function $f(h)$. This approach is particularly attractive when only a small number of c_l dominate the representation, but requires that the local state domain H is mapped into the interval over which the basis function is orthogonal and orthogonality relationship has a weighting function equal to one, i.e., $w(h) = 1$. Two potential orthonormal bases that meet these criteria are Legendre polynomials and Fourier series [74–76].

Applying this discretization approach to capture the h dependence in functions $m(h,x,t)$ and $\alpha(h,x,t)$ in Eq. (12), selecting basis functions with $w(h) = 1$

and mapping the local state space to the orthogonal domain leads to the following discretized versions:

$$\frac{1}{\Delta x \Delta t} \int_s \int_n m(h, x, t) dx dt = \sum_{l=0}^{L-1} m[l, s, n] \xi_l(h) \tag{23}$$

$$\frac{1}{\Delta x \Delta t} \int_s \int_n \alpha(h, x, t) dx dt = \sum_{l=0}^{L-1} \alpha[l, s, n] \xi_l(h) \tag{24}$$

The introduction of these discretized representations into Eq. (12) produces the exact same MKS formulation as shown previously in Eq. (20), but with a new interpretation of the index l.

In the remainder of this paper, we first demonstrate the viability of the extended MKS framework presented above for process-structure evolution linkages. Furthermore, in conducting this case study, we will explore using the two approaches described above for the discretization of the functions on the local state space form multiscaling in time by extending the length of time step n to match the time domain of the simulation T through a specific case study.

3. Cahn-Hilliard Simulations and MKS Linkage Calibrations

The simulation data as well as the MKS localization linkages used in this case study were generated using the Python library PyMKS [77]. A Cahn-Hilliard simulation is used to generated data for the calibration of the MKS Linkages and services as a reference to compare their performance. The Cahn-Hilliard equation presented earlier in Eq. (1) was solved using the optimized semi-implicit spectral scheme with periodic boundary conditions described by Cheng and Rutenberg [78]. The parameter γ was set equal to 0.2, and the time step for the calibration dataset was set equal to 10^{-2} sec. Two spatial domains with sizes of 100 X 100 and 300 X 300 were used to examine how the different methods scale for larger simulations. The simulations and the MKS Linkages were used on a machine with 8 quad core 1.0 GHz processors and 8 GB of memory.

In the present study, we focus on capturing process-microstructure localization linkage in one large time step (or multistep) using the MKS framework. Note that this differs from the approach was used in the earlier study [48] where it was shown that once the linkage is established for one time step, it can be recursively applied to march forward in time. The earlier study used the time derivative of the concentration as the output response field, whereas in the present study we have used the concentration at the end of 500 time steps as the output response field.

In this study, we explore both the discretization approaches described earlier for the functions on the local state space. The approaches result in two different MKS localization linkages that look alike in their mathematical forms. The linkage referred to as Legendre MKS linkage throughout the remainder of the paper uses the discretization method outlined in Eq. (23) and Eq. (24) with Legendre polynomials as the basis functions. The other linkage uses the discretization method outlined in Eq. (18) and Eq. (19) and is referred to as the Primitive MKS linkage throughout the remainder of this paper. Both models restrict the local state space domain to [-1, 1].

Only the first term in Eq. (20) is used in this work. In prior work [20, 23–26], it was shown that the first term is dominant for problems with low to moderate contrast, which in turn controls the degree of heterogeneity of the response field. In the present problem, this criterion is met within the 500 time steps used in this study. This results in significant computational advantages as the calibration of the first-order MKS localization kernels can be done efficiently by taking advantage of discrete Fourier transforms (DFT) and the convolution theorem [79, 80]. This transformation leads to

$$P[k,n] = \sum_{l} \beta[l,k,n] M[l,k,0] \tag{25}$$

In Eq. (25) $P[k,n]$, $\beta[l,k,n]$ and $M[l,k,0]$ are the DFTs of $p[s,n]$, $\alpha[l,s,n]$ and $m[l,s,n]$ respectively.

With the uncoupled spatial frequency representation shown in Eq. (25), the β terms can be calibrated easily using multiple linear regression techniques. The

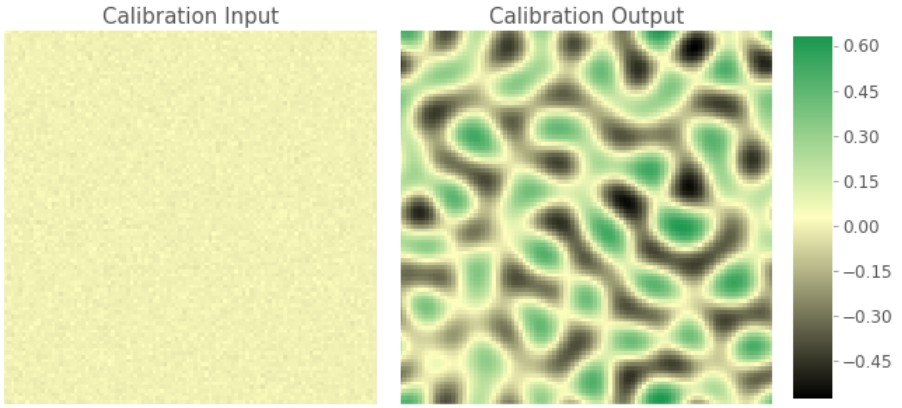

Figure 2: One instance of an initial microstructure (100 x 100) and its corresponding microstructure after 500 time steps, which were used to calibrate the influence coefficients for MKS localization linkages using both the Legendre and the Primitive basis functions.

discretization used for the Primitive MKS linkage is subject to the constraint that the discretized microstructure function sums to one,

$$\sum_{l} m[l, s, n] = 1 \tag{26}$$

therefore multiple linear regression with categorical variables as outlined in previous studies is used [20, 23–25]. The discretized microstructure function in the Legendre MKS linkage is not subject to the constraint shown in Eq. (26) and therefore standard multiple linear regression is used.

The first step in the calibration of MKS localization kernels is the generation of a calibration dataset. For this purpose, Eq. (1) was numerically solved for 500 time steps for 500 randomly generated initial concentration fields with values sampled from a normal distributions with mean values randomly selected between [-0.5, 0.5] and standard deviations of 10^{-2}. The concentration fields at the beginning and the end of the 500 time steps constitute the input and output, respectively for the MKS localization linkage calibration. An example of these fields is shown in Fig. 2. 400 different initial and final (after 500 time steps) concentration fields were generated for calibration.

One of the main MKS parameters for either of the discretization methods is

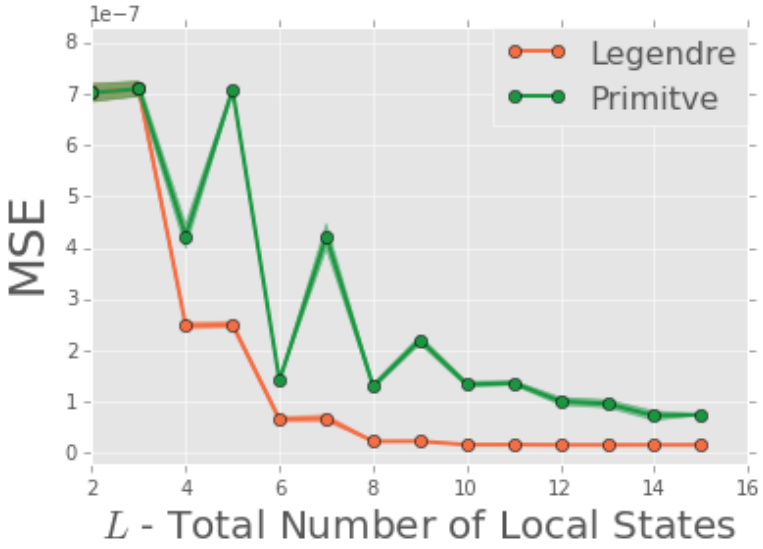

Figure 3: Normalized mean squared error (points) and standard deviation (line widths) values of the predicted concentration fields found using 3-fold cross-validation of MKS localization evolution-linkages using the Legendre and Primitive basis functions to represent the microstructure function and influence function.

the selection of the of total number of local states (or number of basis functions) L used to describe the local state space. In the previous study is was shown that an increase the in variable L can potentially lead to increased accuracy for small time steps at the cost of making the MKS linkage computationally more expensive [48]. The minimum value of L that provides a sufficient level of accuracy is desired.

In order to explore the selection of L for both discretization methods with 1 multistep, the calibration ensemble of data was randomly split into two sets. One set which will be referred to as the linkage selection dataset contains 320 (or 80%) of the microstructures and remaining 80 (or 20%) of the microstructures will be referred to as the linkage validation dataset. In the present work, the two MKS localization linkages were calibrated using the linkage selection dataset while varying L between 2 and 15. In order to avoid over fitting the linkage for a given value of L, 3-fold cross-validation was used. This method randomly

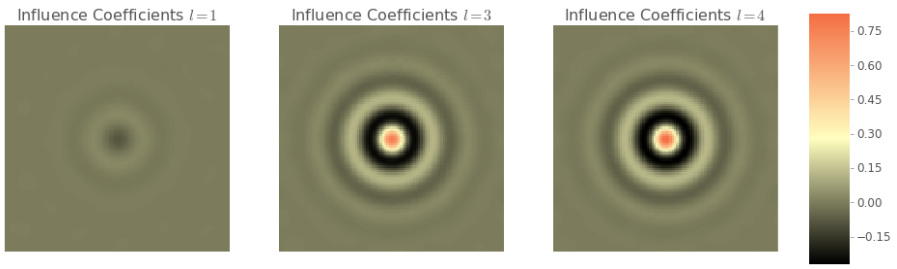

Figure 4: Significant influence coefficients for the Primitive basis for with L equal to 6. All other influence coefficients were less than 10^{-5}.

partitions the linkage selection dataset into three equally sized sub-datasets and calibrates the linkage three times while systematically leaving out each of the sub-datasets once. This method results in three calibrations for each value of L amounting to a total of 84 calibrations between the two MKS localization linkages.

In order to evaluate the accuracy of the linkages while varying L, the mean squared error (MSE) value for each of the calibrations with reference to the Cahn-Hilliard simulation was normalized by the size of the domain and averaged over the ten cross-validation scores. This value is referred to as the normalized MSE value throughout the rest of the paper. The normalized MSE values and their standard deviations are shown in Fig. 3.

The two MKS linkages exhibit an downward overall trend with increasing L. Large and small oscillations were seen in the case of Primitive and Legendre MKS linkages respectively. In the Legendre MKS, it was also observed that the coefficients of the even polynomials in the series were all orders of magnitude smaller than the coefficients of odd polynomials. These observations suggest that the influence functions for the Cahn- Hilliard in Eq. (11) are odd functions. For L greater than 3, the Legendre MKS linkage consistently produced a lower normalized MSE value compared to the corresponding Primitive MKS linkage. It should also be noted that with Primitive basis, the dominant kernels are the ones associated with the important regions in the local state space. With Legendre basis, we get a more organized descriptions of the kernels with the

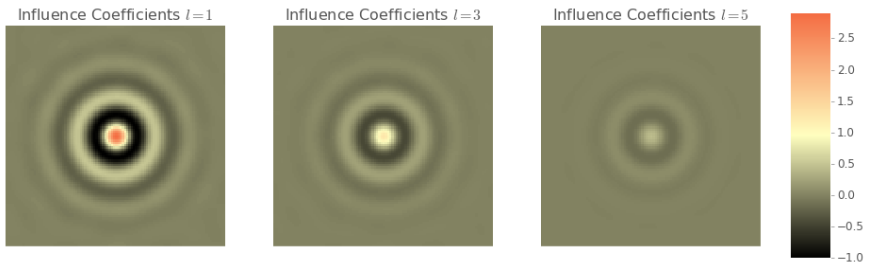

Figure 5: Significant influence coefficients for the Legendre basis with L equal to 6. All other fields had maximum values of less than 10^{-2}.

higher-order terms representing the less important contributions, in general, as one would expect for smooth decaying functions such as the influence functions. Figure 3 shows that $L = 6$ provides sufficiently accurate low-cost linkages that can be used to predict processing-structure evolution for the present case study.

The Primitive and Legendre MKS linkages were both calibrated using the entire calibration dataset with the value of L set equal to 6. These two linkages are used for the remainder of the case study. The discretized influence functions (referred to as influence coefficients) for both linkages can be found on Fig. 4 and Fig. 5.

4. Microstructure Evolution Linkages for Cahn-Hilliard Simulation

Both MKS linkages calibrated in this study were used to predict the microstructure evolution of the same set of 250 initial concentration fields. In order to do this, the initial microstructures, one instance shown in Fig. 6, generated from normal distrubtions with mean values randomly selected between [-0.1, 0.1] and standard deviations of 10^{-2} were used as inputs into the Cahn-Hilliard simulation and the two MKS linkages. An instance of the initial microstructure can be found in Fig. 6. The simulation numerically predicted each of the microstructures after 500 time steps with an average run time of 1.33 seconds. The MKS linkages used the same initial inputs and the predicted microstructures equivalent to running the simulation for 500 time steps, but

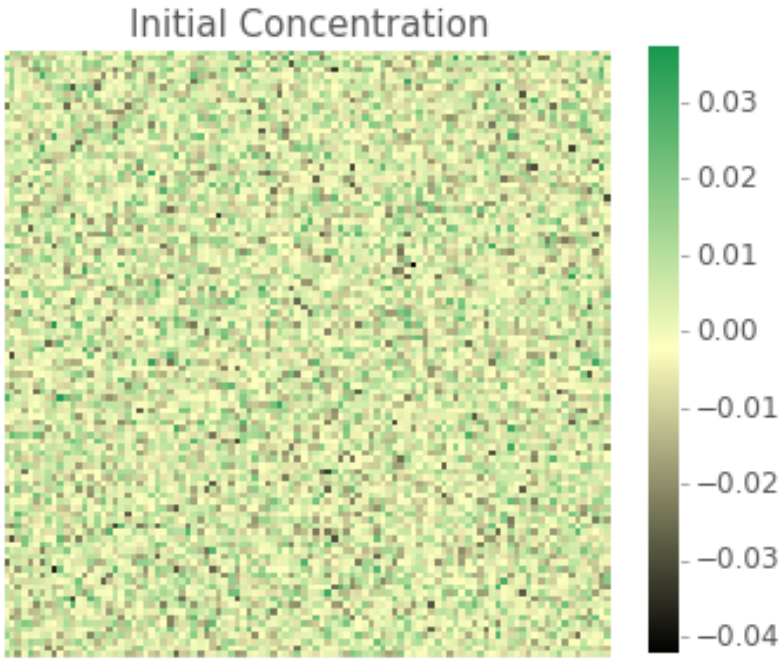

Figure 6: Initial microstructure (100 x 100) used as a common input for the Cahn-Hilliard simulations as well as the MKS localization linkages with Primitive and Legendre basis functions.

with one multistep. The average run time of the Primitive and Legendre MKS linkages were 3.82 x 10^{-3} seconds and 4.94 x 10^{-3} seconds with averaged normalized MSE values of 5.42 x 10^{-7} and 1.61 x 10^{-7} respectively. As a reference the time step of the simulation was changed to match the large multistep used by the MKS linkages and the same initial microstructures were solved with an average run time of 2.51x 10^{-3} and an averaged normalized MSE value of 4.76 x 10^{-6}. An instance of the final predicted microstructures for the MKS linkages and the simulations are compared in Fig. 7.

One of the major advantages of using the MKS localization linkage is that the learning in the form of the MKS influence coefficients (discretized kernels) can be transferred to other initial microstructures that may be defined on larger spatial domains. In other words, the same influence coefficients that are cal-

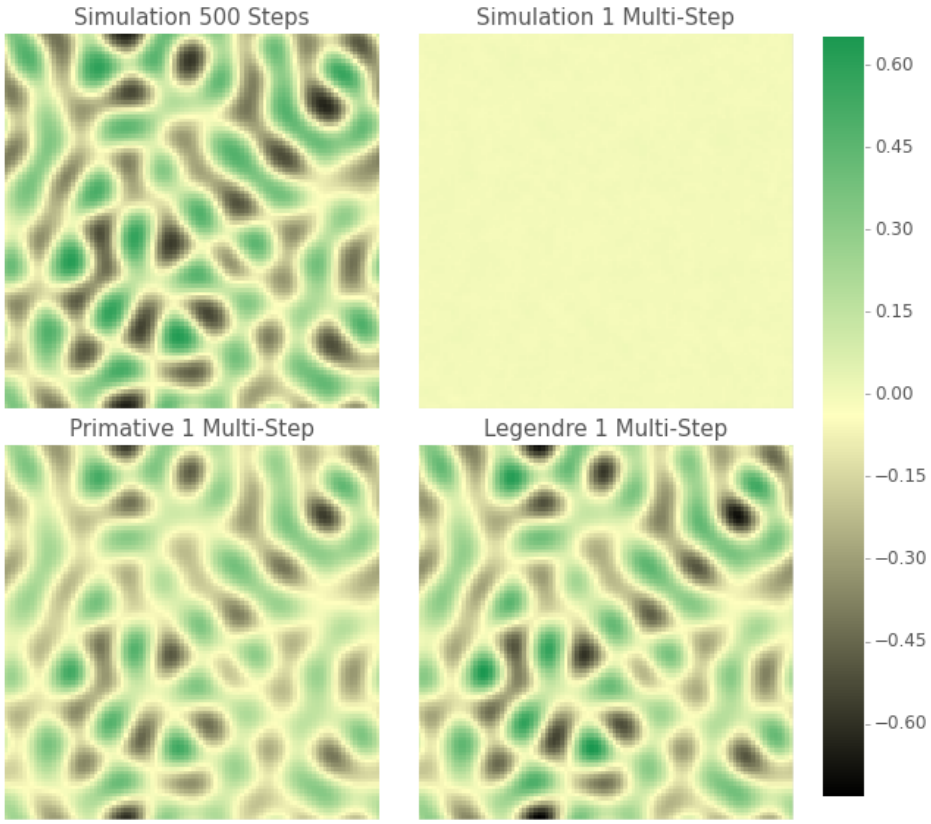

Figure 7: Predicted concentration fields by simulations using 500 time steps and one large multistep (above) as well as the concentration fields predicted by the two MKS localization linkages using one large multistep (below).

ibrated on a small dataset can be used to predict the structure evolution for a much larger microstructures. This allows for the influence coefficients to be calibrated once and used to represent the processing-microstructure evolution for simulations with equal or larger domains sizes. Because of the decaying nature of the discretized influence functions in real space as shown in Fig. 4 and Fig. 5, the edges can be zero padded to expand their domain size to match the domain of new initial microstructure. The influence coefficients for both of the Primitive and the Legendre MKS linkages were scaled up from a domain of size 100 by 100 to 300 by 300 using the method outlined by Landi et al. [24].

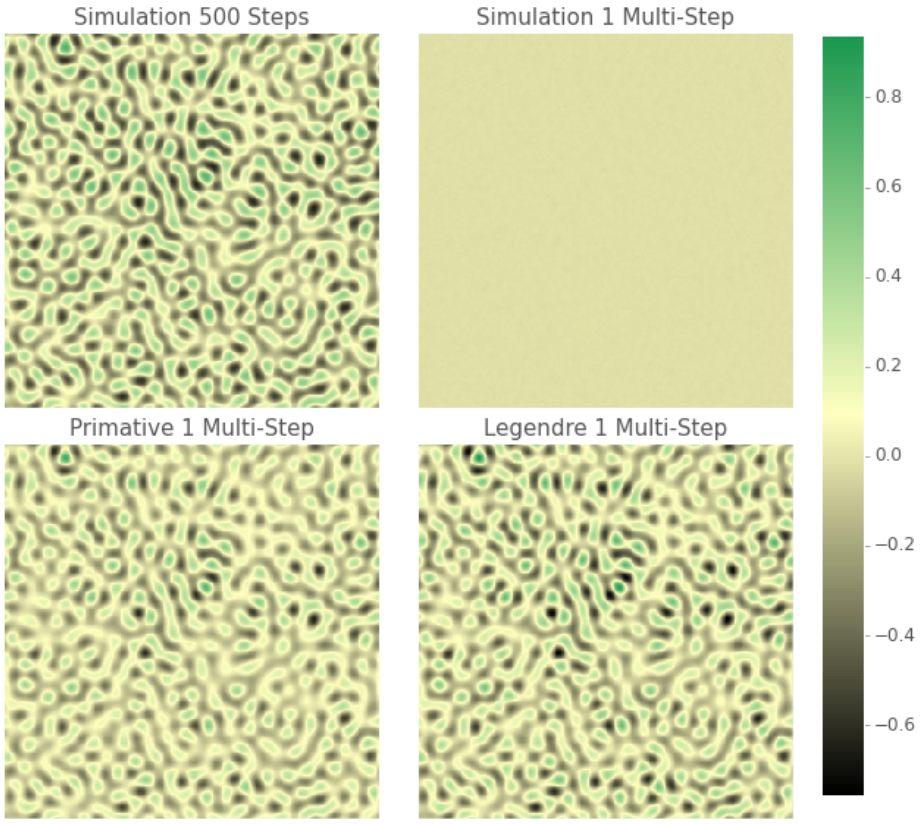

Figure 8: Initial large microstructure (300 x 300) used as a common input for the Cahn-Hilliard simulations and the MKS localization linkages.

A set of 250 initial microstructures were created using the same method as described above, but on a larger spatial domain of 300 x 300, is shown in Fig. 8. These microstructures were used as inputs to the same the Cahn-Hilliard simulations and the MKS localization linkages and the final microstructures were predicted. The average run time for the simulation using 500 time steps was 1.13 x 10^2 seconds. Primitive and Legendre MKS linkages had run times of 3.54 x 10^{-2} seconds and 7.00 x 10^{-2} seconds, with averaged normalized MSE values 5.69 x 10^{-8} and 1.82 x 10^{-8} respectively. The average run time and and averaged normalized MSE value for the simulation with the large time step were 2.31 x 10^{-2} seconds and 6.08 x 10^{-7}. The predicted concentration fields are compared in Fig. 9.

5. Conclusion

A new generalized MKS framework with two different discretization methods for the local state variables has been developed for formulating computationally low-cost process-structure linkages which allow for temporal multiscaling. This framework is quite general and allows compact representation of the influence functions (or kernels) on the local state spaces. The overall framework was presented and demonstrated using a Cahn-Hilliard microstructure evolution as a prime example.

Although the computational cost of the Primitive MKS linkage was slightly lower than the Legendre MKS linkage, and the Legendre MKS linkage was more accurate and showed more stable decay of error with increasing number of terms in the series. Both MKS localization linkages predicted the process-structure evolution for the concentration fields three orders of magnitude faster than the simulation with a small time step, and had averaged normalized MSE values that were an order of magnitude lower than the Cahn-Hilliard simulation with the same large time step.

This case study suggests that MKS localization framework provides an alternate method to learn the underlying embedded physics in a numerical model.

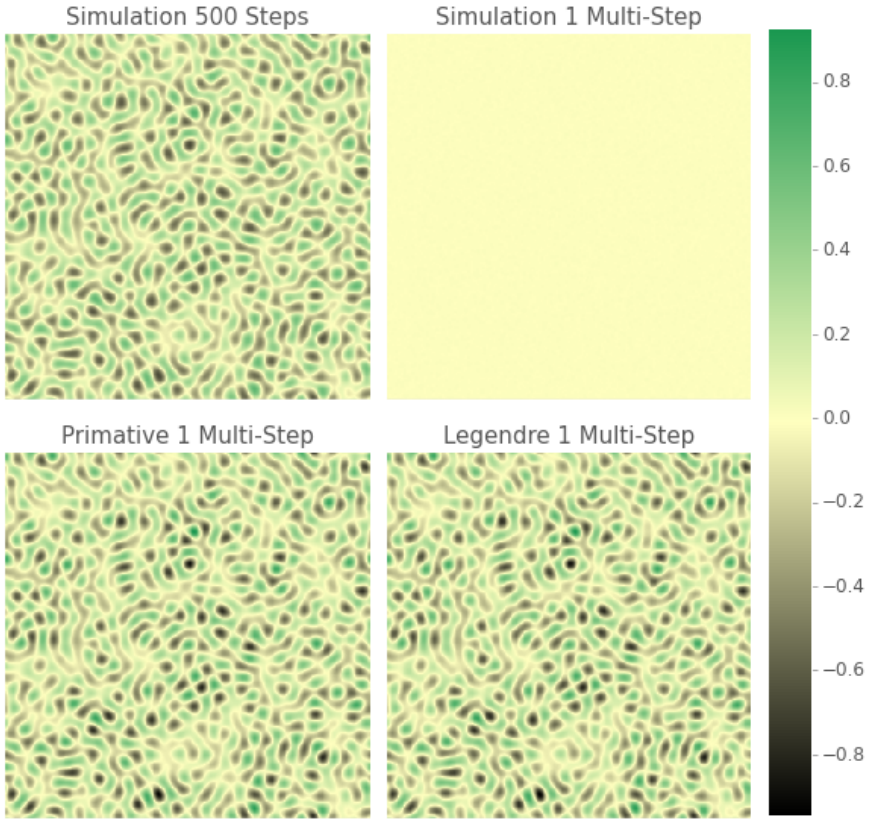

Figure 9: The concentration fields predicted by the numerical simulation with a small time step and with one large multistep (above) as well as the concentration fields predicted by the MKS localization linkages with scaled up influence coefficients from a domain size of 100 by 100 to 300 by 300 with Primitive and Legendre bases(below).

This form of expression of the underlying physics as Green's function based influence kernels (as opposed to expression in the form of differential equations) may provide certain computational advantages in rapid exploration of large spaces in process design to attain desired or specified microstructures. This is especially the case for problems where traditional numerical integration schemes have been difficult to optimize.

Overall, it was demonstrated that the MKS kernels extracted for the example studied were indeed insensitive to the details of the initial microstructure (in other words the same kernel can be applied to any initial microstructure in the selected material system) and could be trivially expanded for applications to larger domain sizes with comparable accuracy. The method described here has laid a strong foundation for future developments addressing a broad range of materials systems with richer microstructures and more complex governing physics.

6. Acknowledgements

DBB and SRK acknowledge support from NIST 70NANB14H191.

References

[1] C. Ward, Materials genome initiative for global competitiveness, in: 23rd Advanced Aerospace Materials and Processes (AeroMat) Conference and Exposition, Asm, 2012.

[2] J. Allison, D. Backman, L. Christodoulou, Integrated computational materials engineering: a new paradigm for the global materials profession, JOM 58 (11) (2006) 25–27.

[3] National Science and Technology Council Executive Office of the President, Materials genome initiative for global competitiveness (2011).
URL http://www.whitehouse.gov/sites/default/files/microsites/ostp/materials_genome_initiative-final.pdf

[4] Materials Genome Initiative National Science and Technology Council Committee on Technology Subcommittee on the Materials Genome Initiative, Materials genome initiative strategic plan (2014).
URL http://www.whitehouse.gov/sites/default/files/microsites/ostp/NSTC/mgi_strategic_plan_-_dec_2014.pdf

[5] J. Allison, Integrated computational materials engineering: A perspective on progress and future steps, JOM Journal of the Minerals, Metals and Materials Society 63 (4) (2011) 15–18.

[6] G. B. Olson, Designing a new material world, Science 288 (5468) (2000) 993–998.

[7] N. R. C. U. C. on Integrated Computational Materials Engineering, Integrated computational materials engineering: a transformational discipline for improved competitiveness and national security, National Academies Press, 2008.

[8] G. J. Schmitz, U. Prahl, Integrative computational materials engineering: Concepts and applications of a modular simulation platform, John Wiley & Sons, 2012.

[9] L. Robinson, Tms study charts a course to successful icme implementation (2013).

[10] J. E. Allison, Integrated computational materials engineering (icme): A transformational discipline for the global materials profession, Metals and Materials 223.

[11] A Study Organized by The Minerals, Metals & Materials Society, Integrated computational materials engineering (icme): Implementing icme in the aerospace, automotive, and maritime industries (2013).

[12] M. J. Buehler, A. Hartmaier, H. Gao, Hierarchical multi-scale modelling of plasticity of submicron thin metal films, Modelling And Simulation In Materials Science And Engineering 12 (4) (2004) S391.

[13] S. Groh, E. Marin, M. Horstemeyer, H. Zbib, Multiscale modeling of the plasticity in an aluminum single crystal, International Journal of Plasticity 25 (8) (2009) 1456–1473.

[14] D. J. Luscher, D. L. McDowell, C. A. Bronkhorst, A second gradient theoretical framework for hierarchical multiscale modeling of materials, International Journal of Plasticity 26 (8) (2010) 1248–1275.

[15] J. T. Oden, K. Vemaganti, N. Moës, Hierarchical modeling of heterogeneous solids, Computer Methods in Applied Mechanics and Engineering 172 (1) (1999) 3–25.

[16] D. L. McDowell, A perspective on trends in multiscale plasticity, International Journal of Plasticity 26 (9) (2010) 1280–1309.

[17] G. B. Olson, Computational design of hierarchically structured materials, Science 277 (5330) (1997) 1237–1242.

[18] J. H. Panchal, S. R. Kalidindi, D. L. McDowell, Key computational modeling issues in integrated computational materials engineering, Computer-Aided Design 45 (1) (2013) 4–25.

[19] M. Shenoy, Y. Tjiptowidjojo, D. McDowell, Microstructure-sensitive modeling of polycrystalline in 100, International Journal of Plasticity 24 (10) (2008) 1694–1730.

[20] H. F. Al-Harbi, G. Landi, S. R. Kalidindi, Multi-scale modeling of the elastic response of a structural component made from a composite material using the materials knowledge system, Modelling and Simulation in Materials Science and Engineering 20 (5) (2012) 055001.

[21] The Minerals Metals & Materials Society (TMS), Modeling Across Scales: A Roadmapping Study for Connecting Materials Models and Simulations Across Length and Time Scales, TMS, Warrendale, PA, 2015. doi:10.7449/multiscale_1.
URL www.tms.org/multiscalestudy

[22] S. R. Kalidindi, Data science and cyberinfrastructure: critical enablers for accelerated development of hierarchical materials, International Materials Reviews 60 (3) (2015) 150–168.

[23] S. R. Kalidindi, S. R. Niezgoda, G. Landi, S. Vachhani, T. Fast, A novel framework for building materials knowledge systems, Computers, Materials, & Continua 17 (2) (2010) 103–125.

[24] G. Landi, S. R. Niezgoda, S. R. Kalidindi, Multi-scale modeling of elastic response of three-dimensional voxel-based microstructure datasets using novel dft-based knowledge systems, Acta Materialia 58 (7) (2010) 2716–2725.

[25] Y. C. Yabansu, D. K. Patel, S. R. Kalidindi, Calibrated localization relationships for elastic response of polycrystalline aggregates, Acta Materialia 81 (2014) 151–160.

[26] Y. C. Yabansu, S. R. Kalidindi, Representation and calibration of elastic localization kernels for a broad class of cubic polycrystals, Acta Materialia 94 (2015) 26–35.

[27] E. Kröner, Statistical modelling, in: Modelling small deformations of polycrystals, Springer, 1986, pp. 229–291.

[28] E. Kröner, Bounds for effective elastic moduli of disordered materials, Journal of the Mechanics and Physics of Solids 25 (2) (1977) 137–155.

[29] D. B. Suits, Use of dummy variables in regression equations, Journal of the American Statistical Association 52 (280) (1957) 548–551.

[30] F. Galton, Regression towards mediocrity in hereditary stature., Journal of the Anthropological Institute of Great Britain and Ireland (1886) 246–263.

[31] J. W. Cooley, J. W. Tukey, An algorithm for the machine calculation of complex fourier series, Mathematics of computation 19 (90) (1965) 297–301.

[32] V. Volterra, Theory of functionals and of integral and integro-differential equations, Courier Corporation, 2005.

[33] H. Bunge, C. Esling, Texture development by plastic deformation, Scripta metallurgica 18 (3) (1984) 191–195.

[34] S. R. Kalidindi, H. K. Duvvuru, M. Knezevic, Spectral calibration of crystal plasticity models, Acta Materialia 54 (7) (2006) 1795–1804.

[35] J. B. Shaffer, M. Knezevic, S. R. Kalidindi, Building texture evolution networks for deformation processing of polycrystalline fcc metals using spectral approaches: applications to process design for targeted performance, International Journal of Plasticity 26 (8) (2010) 1183–1194.

[36] M. Knezevic, A. Levinson, R. Harris, R. K. Mishra, R. D. Doherty, S. R. Kalidindi, Deformation twinning in az31: influence on strain hardening and texture evolution, Acta Materialia 58 (19) (2010) 6230–6242.

[37] H. F. Al-Harbi, M. Knezevic, S. R. Kalidindi, Spectral approaches for the fast computation of yield surfaces and first-order plastic property closures for polycrystalline materials with cubic-triclinic textures, Computers, Materials, & Continua 15 (2) (2010) 153–172.

[38] H. K. Duvvuru, M. Knezevic, R. K. Mishra, S. R. Kalidindi, Application of microstructure sensitive design to fcc polycrystals, in: Materials science forum, Vol. 546, Trans Tech Publ, 2007, pp. 675–680.

[39] D. Li, H. Garmestani, S. Schoenfeld, Evolution of crystal orientation distribution coefficients during plastic deformation, Scripta Materialia 49 (9) (2003) 867–872.

[40] D. Li, H. Garmestani, B. Adams, A texture evolution model in cubic-orthotropic polycrystalline system, International journal of plasticity 21 (8) (2005) 1591–1617.

[41] D. Li, H. Garmestani, S. Ahzi, Processing path optimization to achieve desired texture in polycrystalline materials, Acta materialia 55 (2) (2007) 647–654.

[42] D. S. Li, J. Bouhattate, H. Garmestani, Processing path model to describe texture evolution during mechanical processing, in: Materials Science Forum, Vol. 495, Trans Tech Publ, 2005, pp. 977–982.

[43] A. Creuziger, L. Hu, T. Gnäupel-Herold, A. D. Rollett, Crystallographic texture evolution in 1008 steel sheet during multi-axial tensile strain paths, Integrating Materials and Manufacturing Innovation 3 (1) (2014) 1.

[44] V. Sundararaghavan, N. Zabaras, A multi-length scale sensitivity analysis for the control of texture-dependent properties in deformation processing, International Journal of Plasticity 24 (9) (2008) 1581–1605.

[45] V. Sundararaghavan, N. Zabaras, Linear analysis of texture–property relationships using process-based representations of rodrigues space, Acta materialia 55 (5) (2007) 1573–1587.

[46] S. K. Samudrala, J. Zola, S. Aluru, B. Ganapathysubramanian, Parallel framework for dimensionality reduction of large-scale datasets, Scientific Programming.

[47] K. Chang, C. E. Krill III, Q. Du, L.-Q. Chen, Evaluating microstructural parameters of three-dimensional grains generated by phase-field simulation or other voxel-based techniques, Modelling and Simulation in Materials Science and Engineering 20 (7) (2012) 075009.

[48] T. Fast, S. R. Niezgoda, S. R. Kalidindi, A new framework for computationally efficient structure–structure evolution linkages to facilitate high-fidelity scale bridging in multi-scale materials models, Acta Materialia 59 (2) (2011) 699–707.

[49] M. Cheng, J. A. Warren, Controlling the accuracy of unconditionally stable algorithms in the cahn-hilliard equation, Physical Review E 75 (1) (2007) 017702.

[50] L.-Q. Chen, Phase-field models for microstructure evolution, Annual review of materials research 32 (1) (2002) 113–140.

[51] Z. Bi, R. F. Sekerka, Phase-field model of solidification of a binary alloy, Physica A: Statistical Mechanics and its Applications 261 (1) (1998) 95–106.

[52] S. Torquato, Effective stiffness tensor of composite mediai. exact series expansions, Journal of the Mechanics and Physics of Solids 45 (9) (1997) 1421–1448.

[53] B. L. Adams, S. R. Kalidindi, D. T. Fullwood, Microstructure sensitive design for performance optimization, 2012.

[54] S. R. Kalidindi, M. Binci, D. Fullwood, B. L. Adams, Elastic properties closures using second-order homogenization theories: case studies in composites of two isotropic constituents, Acta materialia 54 (11) (2006) 3117–3126.

[55] D. T. Fullwood, B. L. Adams, S. R. Kalidindi, A strong contrast homogenization formulation for multi-phase anisotropic materials, Journal of the Mechanics and Physics of Solids 56 (6) (2008) 2287–2297.

[56] Y.-P. Pellegrini, Self-consistent effective-medium approximation for strongly nonlinear media, Physical Review B 64 (13) (2001) 134211.

[57] Y.-P. Pellegrini, M. Barthélémy, Self-consistent effective-medium approximations with path integrals, Physical Review E 61 (4) (2000) 3547.

[58] V. Monchiet, G. Bonnet, A polarization-based fft iterative scheme for computing the effective properties of elastic composites with arbitrary contrast,

International Journal for Numerical Methods in Engineering 89 (11) (2012) 1419–1436.

[59] V. Monchiet, G. Bonnet, Numerical homogenization of nonlinear composites with a polarization-based fft iterative scheme, Computational Materials Science 79 (2013) 276–283.

[60] H. Moulinec, F. Silva, Comparison of three accelerated fft-based schemes for computing the mechanical response of composite materials, International Journal for Numerical Methods in Engineering 97 (13) (2014) 960–985.

[61] F. Willot, B. Abdallah, Y.-P. Pellegrini, Fourier-based schemes with modified green operator for computing the electrical response of heterogeneous media with accurate local fields, International Journal for Numerical Methods in Engineering 98 (7) (2014) 518–533.

[62] B. L. Adams, X. C. Gao, S. R. Kalidindi, Finite approximations to the second-order properties closure in single phase polycrystals, Acta Materialia 53 (13) (2005) 3563–3577.

[63] D. Fullwood, B. Adams, S. Kalidindi, Generalized pareto front methods applied to second-order material property closures, Computational Materials Science 38 (4) (2007) 788–799.

[64] N. Young, An introduction to Hilbert space, Cambridge university press, 1988.

[65] P. R. Halmos, P. R. Halmos, P. R. Halmos, P. R. Halmos, H. Mathematician, Introduction to Hilbert space and the theory of spectral multiplicity, Chelsea New York, 1957.

[66] W. Rudin, Real and complex analysis, Tata McGraw-Hill Education, 1987.

[67] G. B. Folland, Fourier analysis and its applications, Vol. 4, American Mathematical Soc., 1992.

[68] A. V. Oppenheim, R. W. Schafer, J. R. Buck, et al., Discrete-time signal processing, Vol. 2, Prentice-hall Englewood Cliffs, 1989.

[69] S. K. Mitra, Y. Kuo, Digital signal processing: a computer-based approach, Vol. 2, McGraw-Hill New York, 2006.

[70] G. B. Arfken, H. J. Weber, D. Spector, Mathematical methods for physicists, American Journal of Physics 67 (2) (1999) 165–169.

[71] A. Zettl, Sturm-Liouville Theory, Vol. 121, American Mathematical Soc., 2010.

[72] J. Weidmann, Spectral theory of ordinary differential operators, Springer, 1987.

[73] M. Al-Gwaiz, Sturm-Liouville theory and its applications, Springer, 2007.

[74] R. M. Redheffer, R. M. Young, Completeness and basis properties of complex exponentials, Transactions of the American Mathematical Society 277 (1) (1983) 93–111.

[75] E. D. Rainville, Special functions, New York, 1960.

[76] G. B. Arfken, Mathematical methods for physicists, Academic press, 2013.

[77] D. Wheeler, D. Brough, T. Fast, S. Kalidindi, A. Reid, PyMKS: Materials Knowledge System in Python.
URL http://dx.doi.org/10.6084/m9.figshare.1015761

[78] M. Cheng, A. D. Rutenberg, Maximally fast coarsening algorithms, Phys. Rev. E 72 (2005) 055701. doi:10.1103/PhysRevE.72.055701.
URL http://link.aps.org/doi/10.1103/PhysRevE.72.055701

[79] R. Bracewell, The fourier transform and iis applications, New York.

[80] E. O. Brigham, E. Brigham, The fast Fourier transform and its applications, Vol. 1, Prentice Hall Englewood Cliffs, NJ, 1988.